Journal of Sound and Vibration (1987) **116**(2), 239–263

A FINITE ELEMENT SCHEME FOR ATTENUATION IN DUCTS LINED WITH POROUS MATERIAL: COMPARISON WITH EXPERIMENT

R. J. ASTLEY

Department of Mechanical Engineering, University of Canterbury, Christchurch, New Zealand

AND

A. CUMMINGS

Department of Mechanical and Aerospace Engineering, University of Missouri-Rolla, Rolla, Missouri 65401, *U.S.A.*

(*Received* 23 *April* 1986, *and in revised form* 19 *September* 1986)

A general finite element formulation for analysis of the sound field in a uniform flow duct with a bulk-reacting porous liner is given. Numerical results on rectangular ducts lined on all four sides are shown, and some of the lower order acoustic modes are described. Comparison is made between numerically predicted and measured values of modal axial attenuation rate, phase speed and transverse pressure profile both with and without mean airflow. Generally good agreement between prediction and measurement is observed.

1. INTRODUCTION

"Bulk reacting" duct liners are used in a variety of situations to absorb sound: a common application is in the exhaust silencers of internal combustion engines and another is in air conditioning ductwork.

The application of particular interest in the present investigation is the use of porous material as a sound absorbing treatment on the inside walls of air conditioning ducts. This method of noise control is very widespread and indeed it is common practice for ductwork manufacturers to fabricate ducts with layers of glass fibre blanket already attached to all the interior surfaces of the duct; ordinarily, this procedure is carried out only with rectangular section ducts. Therefore engineers involved in the acoustical design of air conditioning ducts need at their disposal means of estimating the attenuation characteristics of rectangular ducts lined on all four sides, for internally propagated noise. Since it is known that mean airflow (which is inevitably present in air moving ducts) affects the upstream and downstream attenuation, it is desirable that this should also be taken into account. There are few available methods for finding acoustic attenuation characteristics in rectangular ducts lined on four sides, even with zero airflow. The method which is probably the most commonly used is that given in the ASHRAE 1984 Systems Handbook [1], and this was originated by Vér [2]. Unfortunately no account is taken of the bulk acoustic properties of the lining material in this scheme, aside from a crude correction for bulk density, and no allowance is made for the effects of mean airflow. Not surprisingly perhaps, there has been some doubt about the reliability of predictions made on this basis, and the method cannot be regarded as better than very approximate. There are several prediction methods available for sound attenuation in rectangular ducts treated on two opposite sides with bulk-reacting absorbent (see for example the paper

0022-460X/87/140239+25 $03.00/0

by Cummings [3]). These are essentially based on the theoretical approach of Scott [4], in which the sound fields in the central airway and in the lining material, derived from the respective governing equations, are matched at the interface by appropriate continuity conditions. Uniform mean airflow is readily taken into account in this sort of model. While it is relatively straightforward to obtain analytical solutions for the sound field in ducts lined on two opposite sides (this includes the case of "splitters"), the extension of similar methods to rectangular ducts lined on four sides is not at all easy. The mode functions that describe the sound field in ducts lined on two opposite sides cannot be used in the case of ducts lined on four sides because these functions are not able simultaneously to satisfy the continuity conditions at a porous material/airway interface and within the porous lining, in the same plane.

It would therefore seem that the need for a method of predicting attenuation in ducts lined on all four sides, in the presence of mean airflow, cannot readily be met by an exact solution, and that some kind of approximate method is appropriate. Because of the fairly simple geometry, a finite difference approximation to the governing equations, leading to an eigenvalue problem, could be implemented. At high frequencies, however, the transverse pressure distribution in ducts with bulk-reacting liners can be a rapidly varying function and a fine mesh would probably be required, leading to excessive demands on computer storage. As an alternative, a finite element scheme was chosen here. This has the additional advantage that it can readily be applied to ducts of *any* cross-sectional geometry, which renders it of general applicability.

In this paper, the details of the finite element method are given and numerical solutions are compared to experimentally measured data on modal transverse pressure profiles, modal axial phase speeds and axial decay rates, with and without mean airflow in rectangular section ducts. A series of design charts similar to those given in reference [3] (embodying attenuation per unit length of duct) is given, for a range of duct geometries and flow resistivities of the linear material; the effect of mean airflow is also examined.

2. ANALYSIS

2.1. GEOMETRY AND GOVERNING EQUATIONS

Figure 1 shows the geometry and co-ordinate system which are used in the analysis to follow. A duct of arbitrary cross-section in the x-y plane is lined with porous material of finite and variable thickness as indicated in Figure 1. The outer wall of the duct, denoted by the contour C_0, is assumed to be rigid and impervious. The boundary between

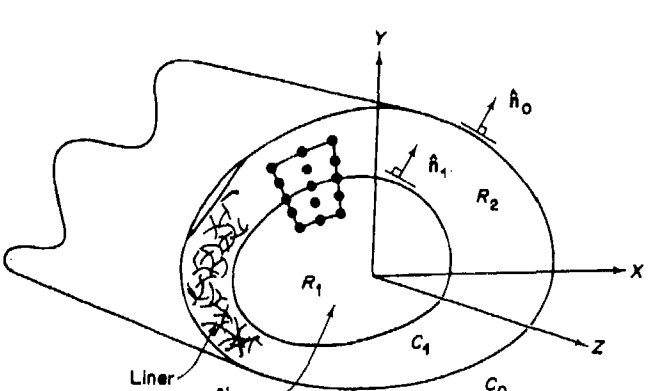

Figure 1. Duct geometry.

the airway, in the centre of the duct, and the porous lining, adjacent to the outer boundary, is represented by the contour C_1. The regions of the duct cross-section occupied by the airway and liner are denoted by R_1 and R_2 respectively. A mean axial airflow of uniform velocity U_0 is present in the airway. It is assumed that the mean airflow in the liner is negligibly small. Coupled acoustical modes which propagate in both the airway and the liner with the same complex axial wavenumber are then sought.

2.1.1. *Governing equations in the airway*

The acoustical pressure and particle displacement in the airway will be denoted by $p_1^*(\mathbf{x}, t)$ and $\boldsymbol{\xi}_1^*(\mathbf{x}, t)$ respectively. The linearized convected acoustical wave equation for a uniformly moving flow then gives

$$\nabla^2 p_1^* = (1/c_0^2)(\partial/\partial t + U_0\,\partial/\partial z)^2 p_1^*, \tag{1}$$

where c_0 is the sound speed and ∇^2 the three dimensional Laplacian operator. A relationship between particle displacement and pressure will also be required when boundary conditions are considered. It is conveniently obtained from the linearized momentum equation which may be written as

$$(\partial/\partial t + U_0\,\partial/\partial z)^2 \boldsymbol{\xi}_1^* = -(1/\rho_0)\nabla p_1^*, \tag{2}$$

(ρ_0 denotes ambient density in the usual notation).

A time harmonic solution, of radian frequency ω, is then sought for an acoustical wave propagating in the airway. The acoustical pressure and particle velocity are accordingly rewritten in the form

$$p_1^*(\mathbf{x}, t) = p_1(x, y)\, e^{i\omega t - ik\lambda z}, \qquad \boldsymbol{\xi}_1(\mathbf{x}, t) = \boldsymbol{\xi}_1(x, y)\, e^{i\omega t - ik\lambda z}. \tag{3}$$

These expressions correspond to an acoustical mode of complex wavenumber $k\lambda$ where $k = \omega/c_0$. If λ is purely real the mode is cut-on in the usual sense. Any imaginary component of λ determines the degree of attenuation.

Equations (1) and (2) then become

$$\nabla^2 p_1 + k^2(1-\lambda M)^2 p_1 - k^2\lambda^2 p_1 = 0, \quad \text{and} \quad k^2(1-\lambda M)^2 \boldsymbol{\xi}_1 = \nabla p_1/\rho_0 c_0^2, \tag{4, 5}$$

where ∇ and $\boldsymbol{\xi}_1$ now denote two dimensional forms—in the x, y plane—of the gradient operator and particle displacement vector respectively and M is the mean flow Mach number U_0/c_0.

2.1.2. *Governing equations in the liner*

The acoustical pressure and particle displacement in the liner (i.e., in the region R_2) will be denoted by $p_2^*(\mathbf{x}, t)$ and $\boldsymbol{\xi}_2^*(\mathbf{x}, t)$. Once again solutions are sought of the form similar to that of expressions (3), i.e.

$$p_2^*(\mathbf{x}, t) = p_2(x, y)\, e^{i\omega t - ik\lambda z}, \qquad \boldsymbol{\xi}_2^*(\mathbf{x}, t) = \boldsymbol{\xi}_2(x, y)\, e^{i\omega t - ik\lambda z}. \tag{6}$$

If the liner is assumed to be homogeneous and isotropic the acoustical behaviour within it may be represented in the absence of flow [5] by the generalized acoustical equation (for simple harmonic time dependence as in equations (6))

$$\nabla^2 p_2^* = (1/c_a^2)\,\partial^2 p_2^*/\partial t^2, \tag{7}$$

where c_a is a complex sound speed incorporating the dissipative effect of the liner. The corresponding momentum equation is

$$\partial^2 \boldsymbol{\xi}_2^*/\partial t^2 = -(1/\rho_a)\nabla p_2^*, \tag{8}$$

where ρ_a is a complex density. Various models are available for determining ρ_a and c_a. One such empirical method will be discussed briefly in the following section. Upon substituting expressions (6) into equations (7) and (8) the resulting two dimensional pressure and momentum equations are:

$$\nabla^2 p_2 + (k_a^2 - k^2\lambda^2)p_2 = 0 \quad \text{and} \quad k_a^2 \xi_2 = \nabla p_2 / c_a^2 \rho_a, \tag{9, 10}$$

where $k_a = \omega / c_a$.

2.1.3. *Bulk properties of the liner*

It will be assumed in the present analysis that the porous liner is both homogeneous and isotropic. This is generally a good first approximation for fibrous liners and plastic foams. Delany and Bazley [6] have shown that for fibrous materials, empirical expressions may be used to represent the characteristic specific impedance ratio $Z_a (= \rho_a c_a / \rho_0 c_0)$ and propagation coefficient $\gamma (= ik_a)$ as functions of a dimensionless parameter $\phi (= \omega\rho_0 / 2\pi\sigma)$ where the parameter σ denotes the steady flow resistivity of the material. The expressions for Z_a and γ proposed in this model take the form

$$Z_a = (1 + c_1 \phi^{c_2}) - i(c_3 \phi^{c_4}) \quad \text{and} \quad \gamma / k = c_5 \phi^{c_6} + i(1 + c_7 \phi^{c_8}). \tag{11a, b}$$

It has been assumed in previous work by one of the authors [3] that similar relationships hold for open-celled plastic foams. This assumption was found to give good results and is used again in the current analysis. The constants c_1 to c_8 must be determined by measurement for specific lining materials (see section 3.1). Although it is an empirical rather than a physical model, the Delany and Bazley approach appears to give good results for a wide range of different liner types.

2.1.4. *Boundary conditions*

Two conditions must be satisfied by the acoustical fields as they match across the interface between the airway and the liner. The first of these requires that the acoustical pressure be continuous across the interface. Since the same values of λ and ω are assumed in expressions (3) and (6) this reduces to the requirement that

$$p_1(x, y) = p_2(x, y) \quad \text{on} \quad C_1. \tag{12}$$

The second condition is the kinematic requirement that the normal component of particle displacement in the airway and the liner must be identical at the interface. In terms of ξ_1 and ξ_2 this may be written

$$\hat{\mathbf{n}}_1 \cdot \xi_1 = \hat{\mathbf{n}} \cdot \xi_2 \quad \text{on} \quad C_1, \tag{13}$$

where $\hat{\mathbf{n}}_1$ is a unit normal on C_1 as indicated in Figure 1. By using equations (5) and (10) this condition may be rewritten in terms of p_1 and p_2 to give

$$(\rho_0 / \rho_a)(1 - \lambda M)^2 \nabla p_2 \cdot \hat{\mathbf{n}}_1 = \nabla p_1 \cdot \hat{\mathbf{n}}_1 \quad \text{on } C_1. \tag{13a}$$

The final boundary condition on the solution is that of zero normal particle displacement at the outer wall. This yields an equivalent pressure condition

$$\nabla p_2 \cdot \hat{\mathbf{n}}_0 = 0 \quad \text{on } C_0, \tag{14}$$

where $\hat{\mathbf{n}}_0$ is a unit outward normal as shown in Figure 1.

The solution of the coupled problem then reduces to the determination, for a given frequency of excitation ω, of the eigenvalues λ which permit the existence of solutions $p_1(x, y)$ and $p_2(x, y)$ to equations (4) and (9) subject to boundary conditions (12), (13a) and (14). Such solutions may conveniently be obtained by expressing the problem in variational form.

2.2. THE VARIATIONAL STATEMENT

The field equations within the liner and airway and the kinematic conditions both at the outer surface of the duct and at the interface between liner and airway may be combined in a single weak variational statement. Consider the complex function χ defined by

$$\chi(p_1, p_2) = \int_{R_1} [\nabla p_1 \cdot \nabla p_1 - k^2(1-\lambda M)^2 p_1^2 + k^2\lambda^2 p_1^2]\, \mathrm{d}R_1 + (\rho_0/\rho_a)(1-\lambda M)^2 \int_{R_2} [\nabla p_2 \cdot \nabla p_2 - k_a^2 p_2^2 + k^2\lambda^2 p_2^2]\, \mathrm{d}R_2. \tag{15}$$

Let p_1 and p_2 belong to a class of continuous functions within R_1 and R_2 which explicitly satisfy the required pressure continuity condition at the liner/airway interface (i.e., $p_1 \equiv p_2$ on C_1). If p_1 and p_2 are permitted to vary by quantities $\varepsilon\eta_1(x, y)$ and $\varepsilon\eta_2(x, y)$ over R_1 and R_2 respectively—where η_1 and η_2 are continuous but otherwise arbitrarily chosen except insofar as the original constraint on p_1 and p_2 must still hold on C_1—the resulting variation in χ is then given by

$$\begin{aligned}\delta\chi &= \chi(p_1+\varepsilon\eta_1, p_2+\varepsilon\eta_2) - \chi(p_1, p_2)\\ &= 2\varepsilon \int_{R_1} [\nabla p_1 \cdot \nabla \eta_1 - k^2(1-\lambda M)^2 p_1\eta_1 + k^2\lambda^2 p_1\eta_1]\, \mathrm{d}R_1\\ &\quad + 2\varepsilon(\rho_0/\rho_a)(1-\lambda M)^2 \int_{R_2} [\nabla p_2 \cdot \nabla \eta_2 - k_a^2 p_2\eta_2 + k^2\lambda^2 p_2\eta_2]\, \mathrm{d}R_2\\ &\quad + \text{terms of order } \varepsilon^2.\end{aligned} \tag{16}$$

The integrals in these expressions may be modified by the use of the divergence theorem to give

$$\begin{aligned}\delta\chi &= -2\varepsilon \int_{R_1} [\nabla^2 p_1 + k^2(1-\lambda M)^2 p_1 - k^2\lambda^2 p_1]\eta_1\, \mathrm{d}R_1\\ &\quad - 2\varepsilon \int_{R_2} [\nabla^2 p_2 + (k_a^2 - k^2\lambda^2)p_2]\eta_2\, \mathrm{d}R_2\\ &\quad + 2\varepsilon \int_{C_1}^{2} [\nabla p_1 \cdot \mathbf{n}_1\eta_1 - (\rho_0/\rho_a)(1-\lambda M)^2 \nabla p_2 \cdot \mathbf{n}_1\eta_2]\, \mathrm{d}s\\ &\quad + 2\varepsilon(\rho_0/\rho_a)(1-\lambda M)^2 \int_{C_0} [\nabla p_2 \cdot \mathbf{n}_0]\eta_2\, \mathrm{d}s + \text{terms of order } \varepsilon^2.\end{aligned} \tag{17}$$

Since η_1 and η_2 are arbitrarily chosen in R_1 and R_2, the first two integrals in expression (17) imply that if χ takes a stationary value, the corresponding functions p_1 and p_2 must satisfy equations (4) and (9) respectively. Similarly since η_1 and η_2 are identical on C_1—having been explicitly chosen so that this is the case—the third integral in expression (17) may be rewritten as

$$\int_{C_1} [\nabla p_1 \cdot \hat{\mathbf{n}}_1 - (\rho_0/\rho_a)(1-\lambda M)^2 \nabla p_2 \cdot \hat{\mathbf{n}}_1]\eta\, \mathrm{d}s, \tag{18}$$

where $\eta = \eta_1 = \eta_2$. Since no other requirement is placed on the choice of η it then follows that the term in square brackets in expression (18) must vanish at all points on C_1 giving boundary condition (13a). Similarly the final integral in expression (17) requires that p_2

satisfies boundary condition (14) on C_0. All of the field equations and boundary conditions required for the solution of the original problem are thus satisfied by those functions p_1 and p_2 giving stationary values of the functional χ subject to the constraint that p_1 and p_2 are identical on the interface C_1. This statement may now be used as the basis for a Rayleigh–Ritz approximate solution. A finite element idealization of the duct cross-section is used to provide suitable basis functions. This procedure is detailed in the following section.

2.3. THE NUMERICAL MODEL

2.3.1. *The finite element discretization*

The variational statement derived in the preceding section is now used to obtain an approximate solution to the original problem by selecting $p_1(x, y)$ and $p_2(x, y)$ from a discrete set of trial functions determined by a finite element subdivision of the duct cross-section. The airway and liner are first subdivided into a number of elements as shown in Figure 1. Nine noded isoparametric Lagrangian rectangles were chosen although other types of element would have been equally suitable. The only constraint on the subdivision is that the contour C_1 must be formed entirely by element boundaries: that is, no element can "straddle" C_1. The resulting nodes are then numbered $1, 2, \ldots, n$ and the corresponding nodal values of p_1 or p_2—depending upon whether the node is in R_1 or R_2—are denoted by $\tilde{p}_1, \tilde{p}_2, \ldots, \tilde{p}_n$. The matrix eigenvalue problem which results from this discretization is simplified somewhat if the nodal points interior to the region R_1 are numbered first—nodes $1, 2, \ldots, r$, say—and those in R_2, including those on C_1, last—nodes $r+1, r+2, \ldots, n$, say. Vectors of nodal values denoted by $\{P_1\}$, $\{P_2\}$ and $\{P\}$ are then defined so that

$$\{P_1\} = \begin{Bmatrix} \tilde{p}_1 \\ \tilde{p}_2 \\ \vdots \\ \tilde{p}_r \end{Bmatrix}, \qquad \{P_2\} = \begin{Bmatrix} \tilde{p}_{r+1} \\ \tilde{p}_{r+2} \\ \vdots \\ \tilde{p}_n \end{Bmatrix} \quad \text{and} \quad \{P\} = \begin{Bmatrix} \tilde{p}_1 \\ \tilde{p}_2 \\ \vdots \\ \tilde{p}_n \end{Bmatrix} = \begin{Bmatrix} P_1 \\ P_2 \end{Bmatrix}. \tag{19}$$

Standard application of the finite element method [7] now yields an implicit trial function, $\tilde{p}$, say, over the entire cross-section given by

$$\tilde{p} = \sum_{i=1}^{n} \tilde{p}_i \psi_i(x, y), \tag{20}$$

where $\psi_i(x, y)$ is the global shape function associated with node i and is defined explicitly within each element by the appropriate element shape function which in this case is a quadratic interpolation function within each element [8]. It should be noted that the above trial function implicitly satisfies the required constraint that $p_1 = p_2$ on C_1, given that the shape functions ψ_i are continuous at all points.

2.3.2. *The matrix eigenvalue problem*

Substitution of expression (20) into the variational functional χ of equation (15) yields a quadratic form, $\tilde{\chi}(\tilde{p}_1, \tilde{p}_2, \ldots, \tilde{p}_n)$ say, of the form

$$\tilde{\chi}(\tilde{p}_1, \tilde{p}_2, \ldots, \tilde{p}_n) = \{p\}^{\mathrm{T}}[A(\lambda)]\{P\}, \tag{21}$$

where

$$\underset{n \times n}{[A(\lambda)]} = [K_1] + (\rho_0/\rho_a)(1 - \lambda M)^2[K_2] - k^2[(1 - \lambda M)^2 - \lambda^2][M_1] - (\rho_0/\rho_a)(1 - \lambda M)^2(k_a^2 - \lambda^2 k^2)[M_2], \tag{22}$$

and the matrices $[K_i]$ and $[M_i]$ $(i=1,2)$ are given by

$$[K_i]_{jk} = \int_{R_i} [(\partial\psi_j/\partial x)(\partial\psi_k/\partial x)+(\partial\psi_j/\partial y)(\partial\psi_k/\partial y)]\,dx\,dy \tag{23}$$

and

$$[M_i]_{jk} = \int_{R_i} [(\psi_j\psi_j)]\,dx\,dy. \tag{24}$$

The stationary values of $\tilde{\chi}$ are then obtained by equating $\partial\tilde{\chi}/\partial\tilde{p}_1 (i=1,\ldots,n)$ to zero giving

$$[A(\lambda)]\{P\} = \{0\}. \tag{25}$$

This non-linear eigenvalue problem ($[A(\lambda)]$ is of fourth order in λ) may then be cast as a linear eigenvalue problem in characteristic form in the following way. First the matrix $[A(\lambda)]$ is rewritten as

$$[A(\lambda)] = [A]+\lambda[B]+\lambda^2[C]+\lambda^3(1/M-\lambda)[D], \tag{26}$$

where the matrices $[A]$, $[B]$, $[C]$ and $[D]$ are independent of λ and are given by

$$[A] = [K_1]+(\rho_0/\rho_a)[K_2]-k^2[M_1]-(\rho_0/\rho_a)k_a^2[M_2], \tag{26a}$$

$$[B] = 2k^2M[M_1]+2k_a^2M(\rho_0/\rho_a)[M_2]-2M(\rho_0/\rho_a)[K_2], \tag{26b}$$

$$[C] = k^2(1-M^2)[M_1]-(\rho_0/\rho_a)(M^2k_a^2-k^2)[M_2]+M^2(\rho_0/\rho_a)[K_2], \tag{26c}$$

$$[D] = -2M^2(\rho_0/\rho_a)k^2[M_2]. \tag{26d}$$

For the case of zero mean flow in the airway ($M=0$) the matrices $[B]$ and $[D]$ are identically zero. Equation (25) then reduces to

$$[[A]+\lambda^2[C]]\{P\} = \{0\}, \tag{27}$$

giving a linear eigenvalue problem of order n for the variable λ^2. The solution of equation (27) then yields eigenvalues λ which occur in complex conjugate pairs indicating, as one would expect in the absence of mean flow, that pairs of eigenmodes result which travel in the positive and negative axial direction with the same phase speed.

When mean flow is present in the airway the matrix eigenvalue problem is somewhat more complicated. It is convenient at this point to partition the matrices $[A]$ and $[B]$ into upper and lower submatrices $[A_1]$, $[A_2]$, $[B_1]$ and $[B_2]$ having r and $(n-r)$ rows respectively: that is, $[A]$ and $[B]$ are written

$$[A] = \begin{bmatrix} A_1 \\ \hline A_2 \end{bmatrix} \quad \text{and} \quad [B] = \begin{bmatrix} B_1 \\ \hline B_2 \end{bmatrix}, \tag{28}$$

where $[A_1]$ and $[B_1]$ are of order $r\times n$, and $[B_2]$ and $[B_3]$ of order $(n-r)\times n$. The matrices $[C]$ and $[D]$ may also be partitioned into submatrices having r and $n-r$ rows and columns, i.e.,

$$[C] = \left[\begin{array}{c|c} C_{11} & C_{12} \\ \hline C_{21} & C_{22} \end{array}\right] \quad \text{and} \quad [D] = \left[\begin{array}{c|c} D_{11} & D_{12} \\ \hline D_{21} & D_{22} \end{array}\right], \tag{29}$$

where $[C_{11}]$ and $[D_{11}]$ are of order $r\times r$, $[C_{12}]$ and $[D_{12}]$ of order $r\times(n-r)$ *et cetera.* One may deduce also from equations (26) and (23) that the matrix $[D]$, when partitioned in this way, has only one non-zero subcomponent, namely $[D_{22}]$. This is the case since the integral required to evaluate the components of $[D]$ (see equation (26d)) involves only an integration over the region R_2 within which the shape functions $\psi_1,\ldots,\psi_r$ are identically zero since they are associated with nodes $1,\ldots,r$ interior to R_1. The original

non-linear eigenvalue problem of equation (24) may therefore be rewritten in partitioned form as

$$\left[\begin{array}{c} A_1 \\ \hline A_2 \end{array}\right]\{P\}+\lambda\left[\begin{array}{c} B_1 \\ \hline B_2 \end{array}\right]\{P\}+\lambda^2\left[\begin{array}{c|c} C_{11} & C_{12} \\ \hline C_{21} & C_{22} \end{array}\right]\left\{\begin{array}{c} P_1 \\ \hline P_2 \end{array}\right\}+\lambda^3(1/M-\lambda)\left[\begin{array}{c|c} 0 & 0 \\ \hline 0 & D_{22} \end{array}\right]\left\{\begin{array}{c} P_1 \\ \hline P_2 \end{array}\right\}=\{0\} \tag{30}$$

or, after further manipulation and rearrangement,

$$\begin{bmatrix} 0 & I & 0 & 0 \\ -C_{11}^{-1}A_1 & -C_{11}^{-1}B_1 & -C_{11}^{-1}C_{12} & 0 \\ 0 & 0 & I & 0 \\ 0 & 0 & 0 & I \\ D_{22}^{-1}[C_{21}C_{11}^{-1}A_1-A_2] & D_{22}^{-1}[C_{21}C_{11}^{-1}B_1-B_2] & D_{22}^{-1}[C_{21}C_{11}^{-1}C_{12}-C_{22}] & -(1/M)I \end{bmatrix}\begin{Bmatrix} P \\ \lambda P \\ \lambda^2 P_2 \\ \lambda^3 P_2 \end{Bmatrix}=\lambda\begin{Bmatrix} P \\ \lambda P_1 \\ \lambda P_2 \\ \lambda^2 P_2 \\ \lambda^3 P_2 \end{Bmatrix}. \tag{31}$$

The solution of equation (25) is then reduced to a linear eigenvalue problem of order $(4n-2r)$. The increase in the order of the problem compared with the no-flow case, for which the eigenmatrix was of order n, is not unexpected. The upstream and downstream propagating modes no longer have the same phase speed or mode shape. This doubles the size of the problem immediately. In addition the presence of flow in the airway introduces "hydrodynamic" modes similar to those encountered in ducts with locally reacting liners [9]. These are neutrally stable hydrodynamic disturbances which are convected with the mean flow—that is, have a phase velocity U_0—but do not contribute to the acoustical pressure field within the airway. They are easily identified in the table of eigenvalues produced by the solution of equation (31) since they are effectively unattenuated and have phase velocity c_0M in the positive z direction. They may be neglected when considering acoustical propagation in the duct.

The practical implementation of the numerical scheme culminating in equations (27) and (31) requires first that the matrices $[M_i]$ and $[K_i]$ $(i=1,2)$ be assembled from the appropriate element contributions. This is done in the usual way [7] after the element submatrices have been obtained from expressions (22) and (23), with nine point Gaussian quadrature being used over each element. The assembled versions of these matrices may then be used to form the matrices $[A]$, $[B]$, $[C]$ and $[D]$ of equations (26) and hence the eigenmatrices of equations (27) or (31). The resolution of the matrix eigenvalue problem itself may then be achieved by a number of standard computational routines. In the present analysis a complex, asymmetric QR routine was used. This produces a complete set of eigenvalues λ_i and corresponding acoustical pressure modes. The attenuation per unit length, A_i, say, of the ith mode is then given by

$$A_i=-8{\cdot}6858\ \mathrm{Im}\,(k\lambda_i) \tag{32}$$

and the phase speed, c_i say, by

$$c_i=\omega/\mathrm{Re}\,(k\lambda_i). \tag{33}$$

Both of these quantities are readily measurable. In the following section a procedure is described for the measurement of A_i and c_i—for selectively excited modes—in an attempt to validate the numerical scheme through a comparison of measured and predicted values.

3. MEASUREMENTS

Two series of experimental tests were conducted, one at the University of Canterbury and the second at the University of Missouri-Rolla. Each involved the use of a test section

of duct that was lined on all four sides with a urethane foam material, and had provision for airflow along the central passage. Both ducts were constructed from chipboard, which was sealed with varnish on the inside. Figure 2 shows schematic diagrams of the ducts; both were similar in construction. The duct at the University of Canterbury had the following dimensions: $L = 3$ m, $t = 49{\cdot}5$ mm, $a = 151$ mm, $b = 101$ mm; it will be referred to as duct I. Duct II (at the University of Missouri-Rolla) had the dimensions: $L = 1{\cdot}83$ m, $t = 17{\cdot}5$ mm, $a = 50$ mm, $b = 38$ mm. In the case of duct I, the airflow was provided by a wind tunnel, which was capable of producing a maximum mean flow Mach number of 0·1 in the duct airway; duct II was fitted with three small centrifugal fans, in series, that provided a fixed mean flow Mach number of 0·053. Most of the tests with mean flow were carried out on duct II. The mean airflow velocity was found by traversing a Pitot-static tube in the exit plane of the duct. A sinusoidal acoustic signal was injected into the ducts by means of source loudspeakers located half-way along the duct axis. In addition to tests on the propagation of acoustic modes in the ducts, measurements of the bulk acoustic properties of the lining materials had to be carried out. Both sets of tests are described in the following sections.

3.1. DUCT LINER PROPERTIES

Two different types of urethane foam were used in ducts I and II and thus the properties of both foams had to be measured for use in the numerical model. The properties required

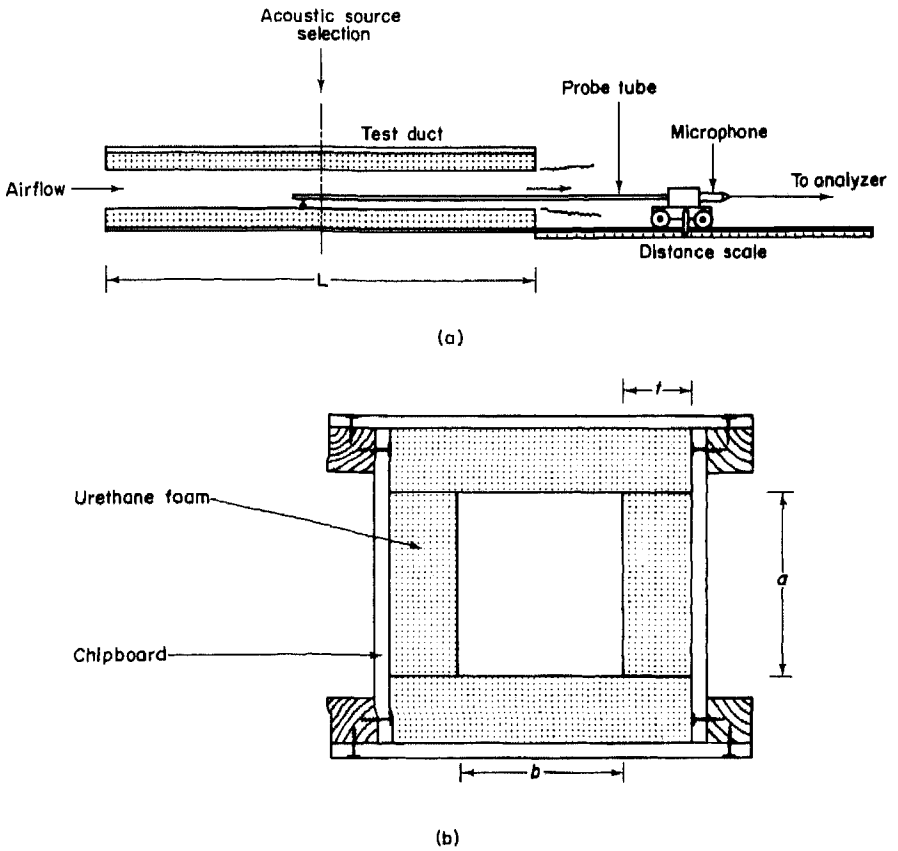

Figure 2. Experimental test arrangement: (a) side view of duct, (b) end view of duct.

were essentially the propagation coefficient γ and the characteristic impedance ratio Z_a; as mentioned in section 2.1.3, both are complex quantities. From these properties, other equivalent parameters can easily be found: for example the complex wavenumber k_a and complex density ρ_a are given in terms of γ and Z_a as follows:

$$k_a = \mathrm{i}\gamma, \qquad \rho_a = -\mathrm{i}\gamma\rho_0 c_0 Z_a/\omega. \tag{34a, b}$$

The method chosen to measure γ and Z_a involved the use of a standing wave tube, in which the non-dimensional impedances (ζ_1 and ζ_2) of two different thicknesses (l_1 and l_2) of the porous material were found, with a rigid backing plate immediately behind the material. Elementary acoustical theory yields expressions for ζ_1 and ζ_2:

$$\zeta_1 = Z_a\,(\coth \gamma l_1), \qquad \zeta_2 = Z_a(\coth \gamma l_2). \tag{35a, b}$$

The characteristic impedance may be eliminated from equations (35), and hence a single equation in γ may be obtained:

$$\zeta_1 \tanh \gamma l_2 - \zeta_2 \tanh \gamma l_1 = 0. \tag{36}$$

From measured values of ζ_1 and ζ_2, together with the known dimensions l_1 and l_2, a solution to this equation may be obtained; then Z_a may be found from either of equations (35). Equation (36) was solved by the Newton–Raphson iterative procedure, and an initial value of γ was found from a simple rigid-frame model of the foam material (see, for example, the book by Morse and Ingard [10]), involving measured values of the steady flow resistivity σ, the volume porosity Ω, and reasonable values of the structure factor and the effective polytropic index of the air in the pores (figures of 2·0 and 1·2 respectively were used). Convergence of the method was rapid and little scatter was found in the resulting data of γ and Z_a. The flow resistivity was found by passing a steady air flow through the porous material and measuring the pressure gradient per unit flow velocity, in the region where viscous stresses govern the flow resistance and the pressure gradient is linearly proportional to flow velocity. The values of σ found for the foams used in ducts I and II were (respectively) 9050 SI rayl/m and 10100 SI rayl/m. From the measured values of γ, Z_a and σ for the two foams, empirical formulae of the aforementioned kind reported by Delany and Bazley [6] were obtained. These formulae have the forms (see equation (11))

$$R = 1 + c_1\phi^{c_2}, \qquad X = -c_3\phi^{c_4}, \qquad \alpha/k = c_5\phi^{c_6}, \qquad \beta/k = 1 + c_7\phi^{c_8}, \tag{37a–d}$$

where $Z_a = R + \mathrm{i}X$ and $\gamma = \alpha + \mathrm{i}\beta$. The measured data involving R, X, α and β were plotted against ϕ on logarithmic scales and the coefficients c_1–c_8 found by fitting straight lines to the data. The values obtained are given in Table 1. The foam used in duct I is termed "pink foam" (because of its colour) and the foam used in duct II is correspondingly termed "yellow foam". The volume porosities of the pink and yellow foams were 0·955 and 0·973 respectively (these figures were obtained from the bulk density of the foam and the density of the solid frame—approximately 1100 kg/m^3).

3.2. SOUND FIELDS IN THE DUCTS

There was a basic difference between the sound source sections used in ducts I and II. In duct I, four small "dome tweeters" were mounted in the vertical walls of the duct, near the corners, so that the chosen modes could be made to propagate within specified frequency ranges. On the other hand duct II incorporated a single, central, sound source consisting of a tube connected to a small acoustic driver; this was designed to cause propagation of the lowest order mode only. Consequently, higher mode propagation measurements were conducted only in duct I.

TABLE 1

Coefficient c_1–c_8 as determined from measured data

	Fibrous material	D12 foam	Pink foam	Yellow foam
c_1	0·0571	0·0794	0·302	0·279
c_2	−0·754	−0·694	−0·322	−0·385
c_3	0·087	0·0665	0·1	0·0881
c_4	−0·732	−0·847	−0·631	−0·799
c_5	0·189	0·153	0·193	0·158
c_6	−0·595	−0·671	−0·505	−0·7
c_7	0·0978	0·174	0·275	0·267
c_8	−0·7	−0·431	−0·359	−0·461

Two types of measurement were carried out on each duct: axial sound pressure traverses, designed to measure the modal attenuation per unit distance and in some cases the axial phase speed, and transverse pressure traverses, intended to measure the pressure distribution across the duct at a particular point. The axial pressure measurements were taken in both ducts I and II by means of a probe tube with the sensing hold in the wall of the tube, and a smoothly pointed tip, to minimize flow separation at the upstream end. In duct I, the sensing hole was located away from either central plane of the duct so that it would not be at a pressure node in the chosen higher order modes. The transverse measurements were also taken by means of a probe tube.

The signal from the probe microphone in both axial and transverse pressure transverses was fed to a frequency analyzer, and—by taking the spectrum—the level and phase of the sinusoidal signal produced by the sound source could thereby be measured independently of the more or less random pressure fluctuations produced by the air flow. In axial traverses, the rate of change of modal sound level with distance, away from the sound source, represented the modal attenuation rate and the rate of phase change, with distance, yielded the modal axial phase speed. Because the sound source was located half-way along the axis of each duct, modal propagation characteristics could be measured for modes propagating against the mean flow—in the section upstream of the source—and with the mean flow, in the section downstream of the source. In the transverse pressure measurements, the acoustic pressure at a series of points on the path of the probe microphone was noted, and a partial description of the modal transverse sound pressure distribution was thus obtained. Modal reflection occurred at the open upstream and downstream duct terminations, but the reflected modes were well attenuated in the central portion of the duct, within about 450 mm on either side of the source section (this applied to both ducts). In order to ensure that the measured data were characteristic of travelling modes, measurements were carried out only in this central region of the test ducts.

The loudspeakers in the source array of duct I were connected so that their phases of motion corresponded to the relative phases in the mode to be excited. Thus (with the speakers assumed to be perfectly matched) only the mode of interest would propagate between its "cut-on frequency" and that of the next mode that could be excited by the speaker arrangement (though the onset of modal cut-on in an absorbing duct is not always sharp). In practice, this method of modal excitation proved to be adequate for the purpose. In duct II, of course, no such provisions were necessary and the single, central sound source excited the lowest order mode sufficiently strongly within the frequency range of interest. The axial attenuation rate of the higher order modes within this range was extremely high and thus modal contamination was not a problem in these tests.

4. RESULTS

The utility of the numerical scheme proposed in section 2 is now demonstrated by a comparison of computed results with those obtained from an alternative analytic approach, for the case of rectangular ducts lined on two sides, and with experimental measurements for the more general case of ducts lined on all sides. Although the numerical scheme itself may be applied without modification to ducts of arbitrary shape—the elements used are isoparametric and do not individually require a rectangular geometry—comparison results are available only for the case of rectangular geometries. All the results presented in this paper are therefore restricted to rectangular cross-section ducts. Most of the results and comparisons are presented for the least attenuated modes present in each duct, these being the most persistent and consequently the most important in practical considerations involving noise attenuation. Some results are, however, presented for higher order modes to demonstrate the validity of the numerical scheme in such cases.

4.1. COMPARISON WITH ANALYTIC RESULTS: RECTANGULAR DUCTS LINED ON TWO SIDES

The case of a rectangular duct lined on two sides has been extensively treated by the second author [3] in a previous study. An analytic solution for this problem may be obtained by reducing it to the solution of a set of coupled ordinary differential equations resulting in a single algebraic eigenvalue relationship. This analysis provides results which are found to correspond well with measured values of attenuation, phase velocity and acoustical pressure distribution in such ducts [3]. The solutions obtained in this way provide a valuable test case for the present scheme since the geometry of such ducts forms a simple subcase of the more general geometry of Figure 1.

Results obtained by using both the analytic scheme of Cummings and the present numerical scheme were compared for a range of duct sizes and liners. Excellent correspondence was established between the two methods. Some typical results are illustrated in Figure 3 in which the predicted attenuation per unit length is plotted for the least attenuated mode in a duct of the dimensions shown (see Figure 3 inset) which is lined with fibrous material of steady flow resistivity 10000 SI rayl/m. The constants c_1–c_8 describing the bulk properties of the liner (see equations (11)) were assumed in both analyses to be those proposed by Delany and Bazley for fibrous materials and are listed in Table 1. The attenuation per unit length is plotted in Figure 3 as a function of frequency for mean flow Mach numbers of −0·2, 0·0 and +0·2. The finite element results were obtained with a four element subdivision of one quarter of the duct cross-section (see inset in Figure 3) although a coarser mesh comprising only two elements gave results (not shown in Figure 3) which were virtually indistinguishable. In all the results to be presented the finite element model utilizes, wherever possible, symmetries present in the geometry of the duct: that is, it is not necessary to model more than one quarter of a rectangular duct with equal liner thicknesses on opposite sides since considerations of symmetry or asymmetry then provide appropriate boundary conditions on the internal boundaries of a single quadrant. For rectangular ducts the least attenuated mode is generally an "even/even" mode for which both the x and y axes act as axes of symmetry. The terms "even/odd" and "odd/even" will similarly refer to modes in which the x axis and y axis (as the case may be) is an axis of symmetry with the remaining axis being an axis of asymmetry. There also exists an "odd/odd" set of modes in which both the x and y axes are axes of asymmetry. These solutions are seldom of interest, being invariably more highly attenuated than the "even/even", "even/odd" or "odd/even" modes.

Returning to the results of Figure 3, one observes that the least attenuated mode in this case was found to be the lowest "even/even" mode and was consequently obtained

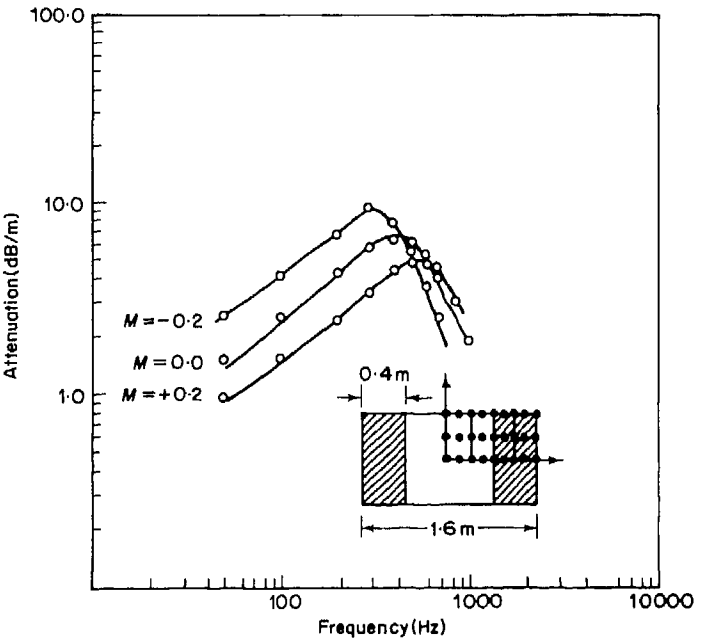

Figure 3. Attenuation per unit length for ducts lined on two sides: ——, analytic, o-computed.

by imposing symmetry about both the x and y axes. The correspondence demonstrated in Figure 3 between results obtained from the present scheme and those of Cummings [3] is reassuringly close. Comparisons of phase velocity and mode shape (not shown) demonstrate a similar degree of correspondence.

Further validation of the finite element scheme is provided in the following section by a comparison of numerical and measured results for the more interesting case of a duct lined on all four sides.

4.2. COMPARISON WITH EXPERIMENT: RECTANGULAR DUCT LINED ON FOUR SIDES

4.2.1. *Zero mean flow*

Results are presented in this section for duct I, with zero mean flow in the airway. The exterior dimensions and liner thickness of the duct are shown in Figure 4 (see inset). Measured values of attenuation, phase speed and pressure distribution for selectively excited modes in this duct were obtained by using the experimental procedures described in section 3. Numerical results were also obtained by using the analysis of section 2. The finite element mesh used to obtain these results is indicated in the inset of Figure 4 and comprises four elements with 25 nodal degrees of freedom. Regular computations were also carried out with a mesh having double this resolution (16 elements and 81 degrees of freedom) as a check on accuracy. Sensibly identical results were obtained in all cases.

A comparison between calculated and measured values of attenuation and phase velocity of the lowest "even/even" mode—for brevity the even/even, even/odd and odd/even modes will be referred to henceforth as (e, e), (e, o) and (o, e) modes—is shown in Figure 4, the predicted values being indicated by the heavy continuous line. The correspondence between measured and predicted values is clearly good for the frequencies shown: that is, less than approximately 1100 Hz. At higher frequencies it becomes difficult to excite a pure (e, e) mode without contamination by higher order modes. The measured values of attenuation and phase velocity then become somewhat erratic and have not

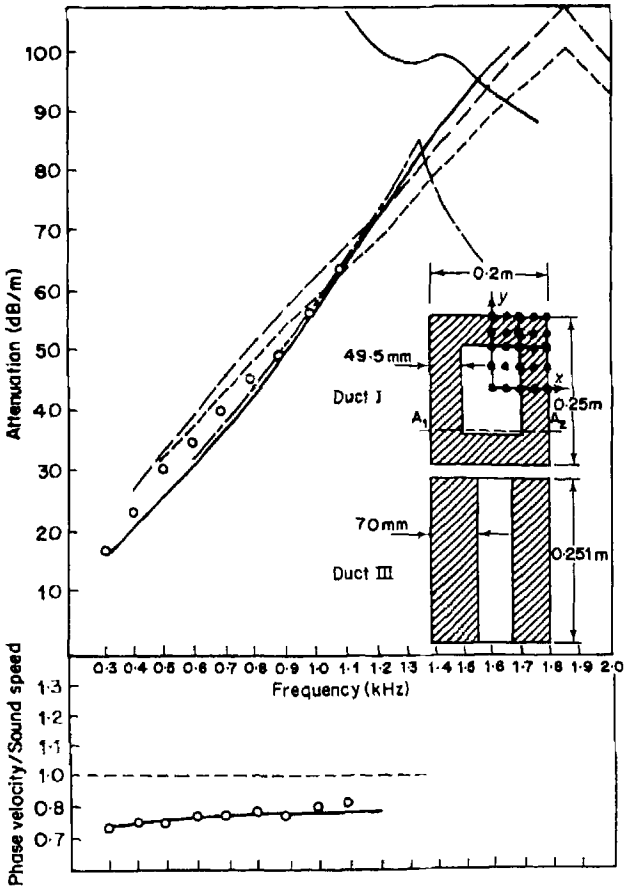

Figure 4. Phase velocity and attenuation for the least attenuated mode. Duct I: ——, computed (pink foam); o, measured (pink foam); - - - - - -, computed (D12 foam); ——— computed (fibrous absorbent). Duct III: — · — · — · —, computed (pink foam).

been included. A typical comparison of predicted and measured pressure mode shapes (at a frequency of 700 Hz) is shown in Figure 5. The experimental values of pressure were measured along a line A_1A_2 (see inset Figure 4) passing through both the airway and the liner. Calculated values were obtained from interpolation along the boundaries of the elements forming this line in the numerical model. Both sets of values are normalized with respect to the acoustical pressure at A_2. This normalization point was chosen since the probe microphone was inserted at A_2 and did not therefore intrude into the duct, being at this stage flush with the wall. Two sets of measured results are shown (for frequencies of 698 and 697 Hz); these exhibit some variation in absolute value—mainly, one suspects, as a consequence of normalization—but are in good general agreement both with each other and with the predicted pressure profile as far as the general shape of the curve is concerned. As one might expect the pressure distribution is a distorted version (the distortion being brought about by the dissipative effect of the liner) of the plane wave which would be present in an unlined duct of the same geometry.

An important feature of the attenuation versus frequency curve of Figure 4—and apparent also in all other curves of this type which are shown—is the presence of a sharp maximum. In this case it occurs at a frequency of approximately 1450 Hz. It is formed by a crossing of the attenuation curves of the first two (e, e) modes. The notation (e, e)

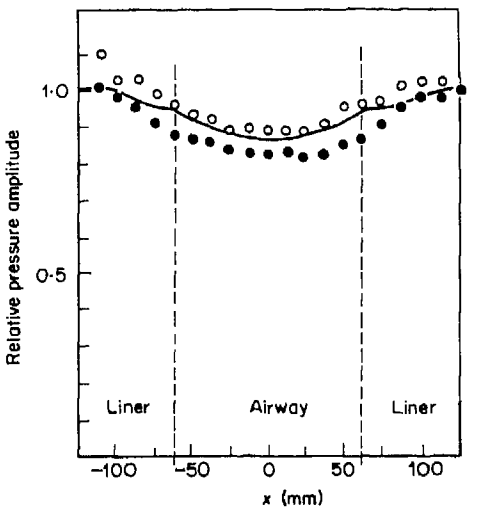

Figure 5. Relative pressure amplitude, Duct I, least attenuated mode, frequency 700 Hz; ——, computed; ●, O, measured.

currently denotes the entire class of even/even modes. In a duct without liners where separable mode numbers m and n may be defined in the x and y directions this class of modes would include all modes (m, n) where m and n were even numbers: that is, modes (0, 0) (0, 2), (2, 0), (2, 2), *et cetera*. This type of classification is of course possible only for the case where the eigenmode is clearly separable into a product of x and y eigenfunctions. In the present case this is not possible and the modes cannot therefore be identified in this precise way although an inspection of their pressure eigenfunctions does sometimes permit their identification as distorted version of their classical (n, m) counterparts. It may easily be deduced, for example, that the monotonically increasing attenuation curve in Figure 4 which approaches the attenuation maximum from the left represents a distorted plane mode. The decreasing curve of attenuation which crosses this line close to 1450 Hz, and subsequently becomes the least attenuated mode itself for frequencies greater than that value, is a higher order mode corresponding to a degenerate form of the (0, 2) or (2, 0)—it is hard to tell which—in an unlined duct. These statements are demonstrated by a sequence (see Figure 6) of computed pressure contours over one quadrant of the duct from the first two modes at frequencies of 1400, 1700 and 2500 Hz. A broken line indicates the airway/liner interface. The predicted pressure amplitude is normalized with respect to its maximum value and plotted in contours at intervals of 0·25. The mode on the left is the least attenuated while that on the right is the next in order of increasing attenuation. The value of the attenuation per unit length for each mode is indicated below each plot. It is one of the advantages of the finite element scheme that such contours are readily accessible from the computed solution and involve little additional computational effort. It is interesting in the light of earlier statements to note the development of these mode shapes as the frequency increases. The distorted plane mode—mode (i) in Figure 6(a), mode (ii) in Figure 6(b) and (c)—has a pressure field which is increasingly confined to the liner with a decreasing relative pressure field in the airway. The pressure gradients in the liner tend to increase the attenuation of this mode and ultimately cause it to lose its position as the least attenuated mode at about 1450 Hz. The "second" (e, e) mode on the other hand (mode (ii) of Figure 6(a) and mode (i) of 6(b) and (c)) has characteristics of hard wall (0, 2) and (2, 0) mode shapes and attains its maximum pressure amplitude

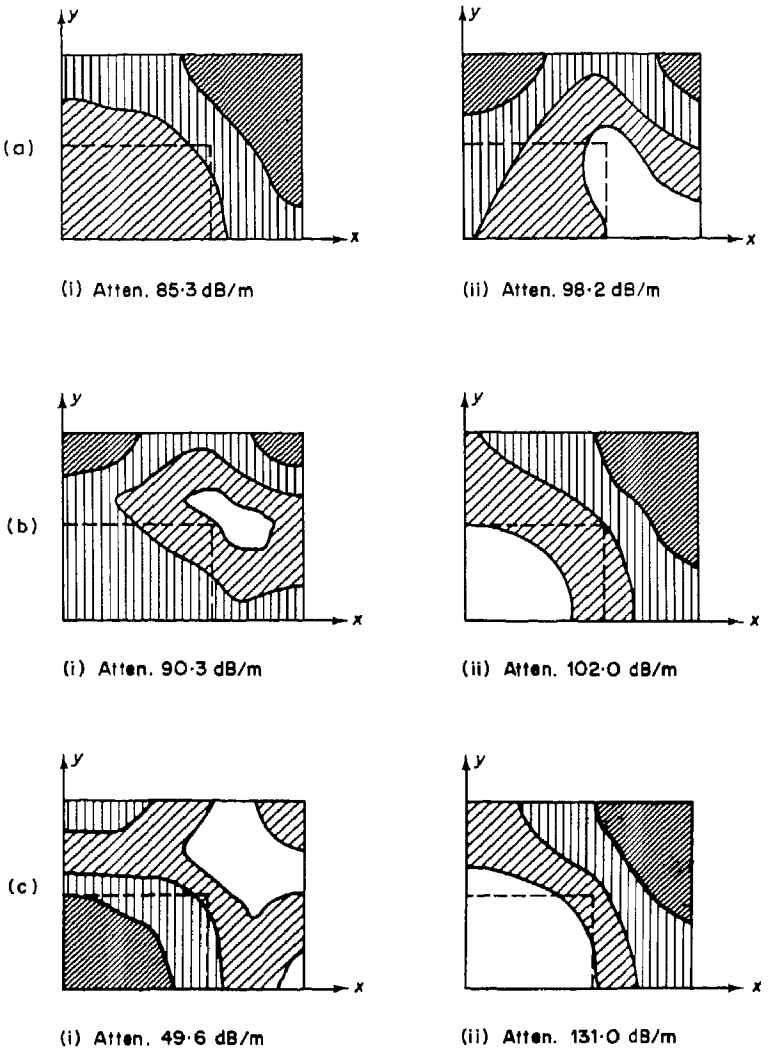

Figure 6. Contours of relative pressure amplitude, Duct I, least attenuated (e, e) modes: (a) frequency 1400 Hz; (b) frequency 1700 Hz; (c) frequency 2500 Hz. □, 0-0·25; ▨, 0·25-0·5; ▥, 0·5-0·75; ▩, 0·75-1·0.

in the airway with a lower-valued, though somewhat more complicated, pressure pattern in the liner. The pressure distribution in the airway tends, in fact, towards a plane wave in that region as the frequency increases while the pressure field in the liner becomes less and less significant in comparison, resulting in decreased overall attenuation. This ultimately leads to this mode becoming the least attenuated mode for frequencies in excess of 1450 Hz. The resulting peak in the attenuation when the two modes cross is clearly an important characteristic of the duct. It is present in much the same form in ducts lined only on two sides as evidenced by the design curves produced for such ducts by Cummings [3]. It is interesting, however, that the present analysis offers some qualitative explanation for the presence of such cusps in terms of the characteristic of the pressure eigenmodes which they represent.

A second—rather elementary—computational exercise, which was carried out in conjunction with Figure 4 was an investigation of the effect on the predicted attenuation of

changes in liner type. The attenuation curves of Figure 4 were accordingly recomputed with different constants $c_1, \ldots, c_8$ being used for the liner properties. The same value of steady flow resistivity was retained (9053 SI rayl/m). The alternative values of the constants $c_1 \ldots . c_8$ which were used were those of Delany and Bazley for fibrous materials and also by those previously obtained by Cummings [3] for a different type of open celled foam ("D12 foam"). Both sets of values are given in Table 1. The resulting attenuation curves are shown in Figure 4 as broken lines. The attenuation peak is shifted upwards in both cases but apart from this the three curves are in relatively close agreement indicating that in many "engineering" applications it may be acceptable to treat bulk liners of diverse materials by using a universal representation of the bulk properties.

A further computational exercise also carried out at this stage and illustrated in Figure 4 was an assessment of the effect of redistributing the same amount of bulk liner on two opposite walls within the same duct. The question to be answered in this case is whether it is more or less advantageous to line all four sides of a duct rather than simply to line two opposite sides. The resulting geometry of an identical duct lined on two sides is shown as DUCT III in Figure 4. The liner thickness on the longer sides is increased from 49·5 mm to 70 mm by a redistribution of that portion of the liner previously attached to the shorter sides. The resulting attenuation curve is included in Figure 4—the liner material is taken to be the same pink foam used to obtain the original (solid line) data—and is seen to give slightly greater attenuation at lower frequencies, as might be expected in view of the increased liner thickness of the longer sides and the essentially plane mode shape at lower frequencies, but to "cross over" to a higher order mode at a lower frequency giving substantially less attenuation as the frequency further increases. The decreased attenuation of this higher order mode is much as one might expect given that reflections from two of the sides are now possible without absorption and that higher order modes, in hard walled ducts at least, may be viewed as the result of interfering plane waves reflecting from the walls. Clearly the attenuation in such ducts benefits overall from the distribution of the liner on all four sides.

The results presented in Figures 4, 5 and 6 all relate to the least attenuated—in this case the lowest (e, e)—mode in the duct. Comparisons of measured and predicted attenuation and phase velocity for higher order modes—the lowest (e, o) and (o, e) modes—are shown in Figures 7 and 8. The measured values were obtained from a selective excitation of these modes, as described in section 3, and the computed values from the same meshes as those of Figure 4 with the appropriate symmetrical or asymmetrical boundary conditions on the x and y axes. The correspondence between measured and predicted attenuation is again good. For the (e, o) mode the phase velocity is also well predicted. For the (o, e) mode this correspondence is less convincing but attributable, the authors suspect, as much to the difficulty of accurately measuring the phase of a highly attenuated mode (that attenuation in this case is in excess of 90 dB/m) than to an inadequacy in the numerical scheme. As with the (e, e) modes the prediction of the pressure eigenmode is in reasonable agreement with measured values, given the requirement for an arbitrary normalization for the purposes of comparison. A typical comparison of measured and predicted relative pressure amplitudes across the line A_1A_2 for the (o, e) mode at frequency of 600 Hz is shown as Figure 9. As with Figure 5 the measured and predicted levels are normalized at A_2. Apart from a slight asymmetry of the measured values the agreement between the two sets of values is good.

Comparisons of this sort, combined with those of the preceding section, lend credence to the belief that the numerical approach is modelling, with reasonable accuracy, the acoustical field within the duct, certainly for the case without flow. When mean flow is present in the airway the comparison with the analytic solutions for ducts lined on two

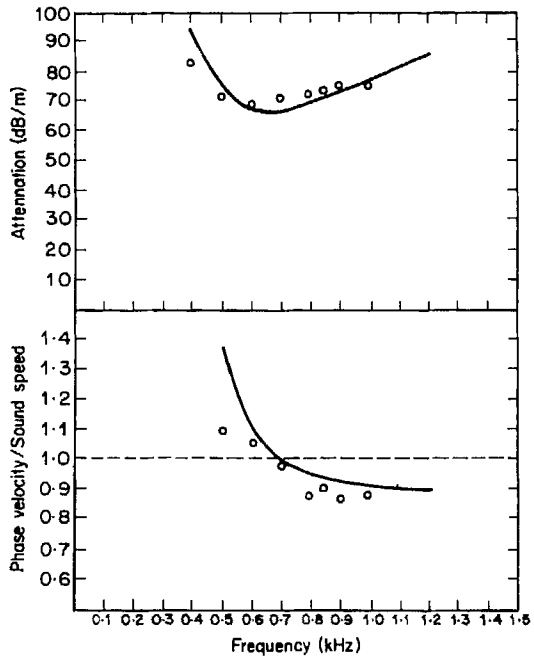

Figure 7. Attenuation per unit length and phase velocity, Duct I, least attenuated (e, o) mode; ——, computed; O, measured.

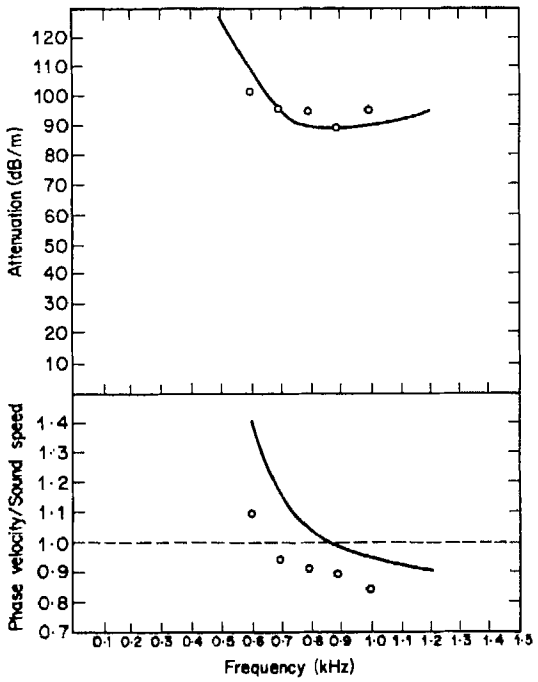

Figure 8. Attenuation per unit length and phase velocity, Duct I, least attenuated (o, e) mode; ——, computed; O, measured.

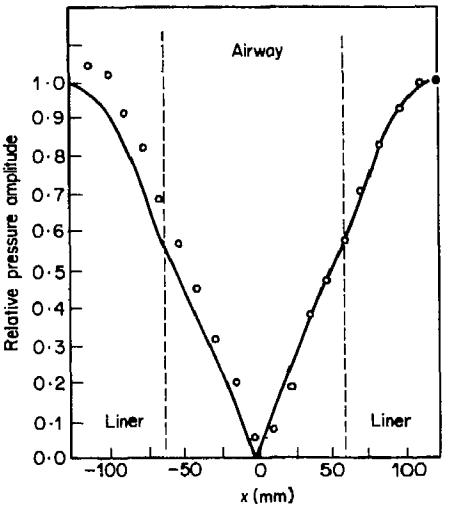

Figure 9. Relative pressure amplitude, Duct I, least attenuated (o, e) mode, frequency 600 H_z; ——, computed; O, measured.

sides only is still good. Comparison between experimental and numerical data for duct II with mean flow is given in the following section.

4.2.2. *Mean flow in airway*

Figure 10 shows the results of modal attenuation tests on the least attenuated (e, e) mode in duct II—with and without mean flow—together with numerical predictions. It can be seen that the finite element scheme is both qualitatively and quantitatively in good agreement with the measurements at frequencies at and below 1 kHz. As expected, the

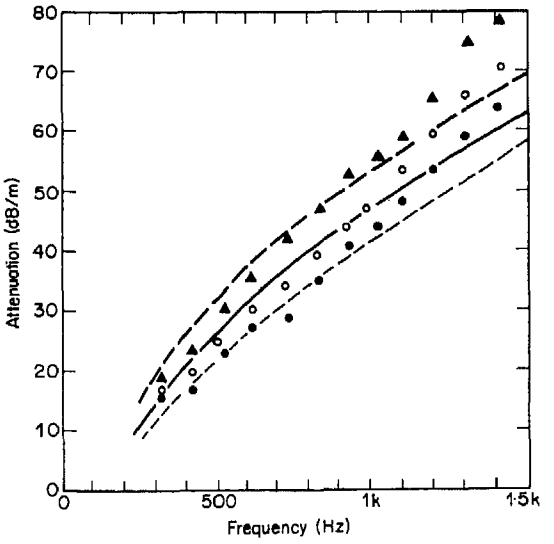

Figure 10. Attenuation of lowest (e, e) mode in Duct II, with and without mean flow; — —, ——, - - - -, computed results for $M = -0{\cdot}053$; $M = 0$, $M = 0{\cdot}053$ respectively; ▲, O, ●, measurements for $M = -0{\cdot}053$, $M = 0$, $M = 0{\cdot}053$ respectively.

mean flow reduces the modal attenuation in the downstream direction and increases the attenuation upstream. Even for this low mean flow Mach number of 0·053, these effects are quite substantial, amounting to about a 50 percent difference between upstream and downstream attenuation at low frequencies.

Above 1·5 kHz, structural vibration in the duct walls, excited by the loudspeaker body, brought about an apparent fall in attenuation with increasing frequency, and data above the frequency were discarded.

Between 1 and 1·5 kHz, the measured data show a consistent trend of being higher than the predicted values, to an increasing extent with rising frequency, though the percentage discrepancies amount to no more than about 20% (a relatively modest amount, in view of the very large range of variation in modal attenuation, with duct dimensions, frequency and porous material properties). The reason for this is not entirely clear, but it is likely to be caused by variations in the thickness of the foam, which amounted to about 1 mm, and variations in the duct dimensions, which were perhaps slightly greater than this. With a duct of such small cross-sectional dimensions, any minor changes in the duct size or the thickness of the porous material are apt to have a much greater effect on modal attenuation than they would have in a larger duct.

At all events, the numerical scheme gives good predictions of the effects of mean flow on the attenuation of the least attenuated (e, e) mode in duct II, as compared to measurements.

5. DESIGN CHARTS FOR DUCT LINERS

The numerical scheme outlined in section 2 was used to determine the attenuation of sound in ducts of various dimensions and liner configurations with a view to providing design information for rectangular air moving ducts lined on all sides. These numerical data are incorporated in a series of charts presented in this section. Initially comprehensive data are presented for square ducts of various sizes in the absence of mean flow. The effects on non-square cross-sections and of mean flow in the airway are then treated in a less detailed fashion.

5.1. PARAMETER SELECTION: DATA FOR SQUARE DUCTS WITHOUT FLOW

In attempting to provide useful design information the data presented must fall short of a complete parametric study, which would involve an enormous number of curves. The approach adopted in this section is similar to that of the second author in his preparation of similar data for ducts lined on two sides only [3]: that is, comprehensive data is presented initially for a limited set of parameters. The effects of variations in some further parameters are then illustrated with reference to some specific cases. In selecting parameters the following characteristics must be represented: (i) duct size and geometry (ii) liner type (iii) the presence or absence of mean flow in the airway.

Initially square ducts only are considered and results are presented for ducts with airways of width 0·1 m, 0·25 m, 0·5 m and 1·0 m. The liner thickness is assumed to be the same on all walls and is quantified by a space factor—defined as airway cross-sectional area divided by total duct cross-sectional area—for which values of 75% and 50%, characteristic of values encountered in air moving ductwork, are selected. The bulk properties of the liner itself must also be incorporated in the presentation of design data. The most commonly used materials in practice are fibrous absorbents of the type modelled by the Delany and Bazley formulas. Numerical results from section 4.2 indicate, moreover, that foam liners, given the same flow resistance, produce attenuation curves which are very similar in general character to those obtained from fibrous liners. All data will

therefore be computed for the case of fibrous liners with the constants $c_1, \ldots, c_8$ being specified by the values of Delany and Bazley (see Table 1). The flow resistivity of the absorbent, which is a useful design parameter since it may often be chosen independently of the other quantities, commonly lies in the range 5000-50 000 SI rayl/m. Data is presented for three specific values spanning this range. These are 10 000, 20 000 and 40 000 SI rayl/m.

In the absence of mean flow the above selection of parameters gives the attenuation curves shown in Figures 11 and 12. The attenuation is calculated for the least attenuated mode propagating in the duct. The mesh used to obtain these results is shown as mesh A (inset) in Figure 11(a). There was some doubt in the author's minds as to the adequacy of this resolution at higher frequencies and check points were therefore calculated with a finer mesh (mesh B of Figure 11(a)). These values are also plotted in Figures 11(a) and 12(a) and clearly differ little from those given by the coarser mesh.

It is noticeable, in both Figures 11 and 12, that some of the attenuation curves do not attain their maxima at a sharp cusp, but in a smooth manner. This is not a draughting error but signifies a continuous transition in the pressure eigenmode rather than an abrupt

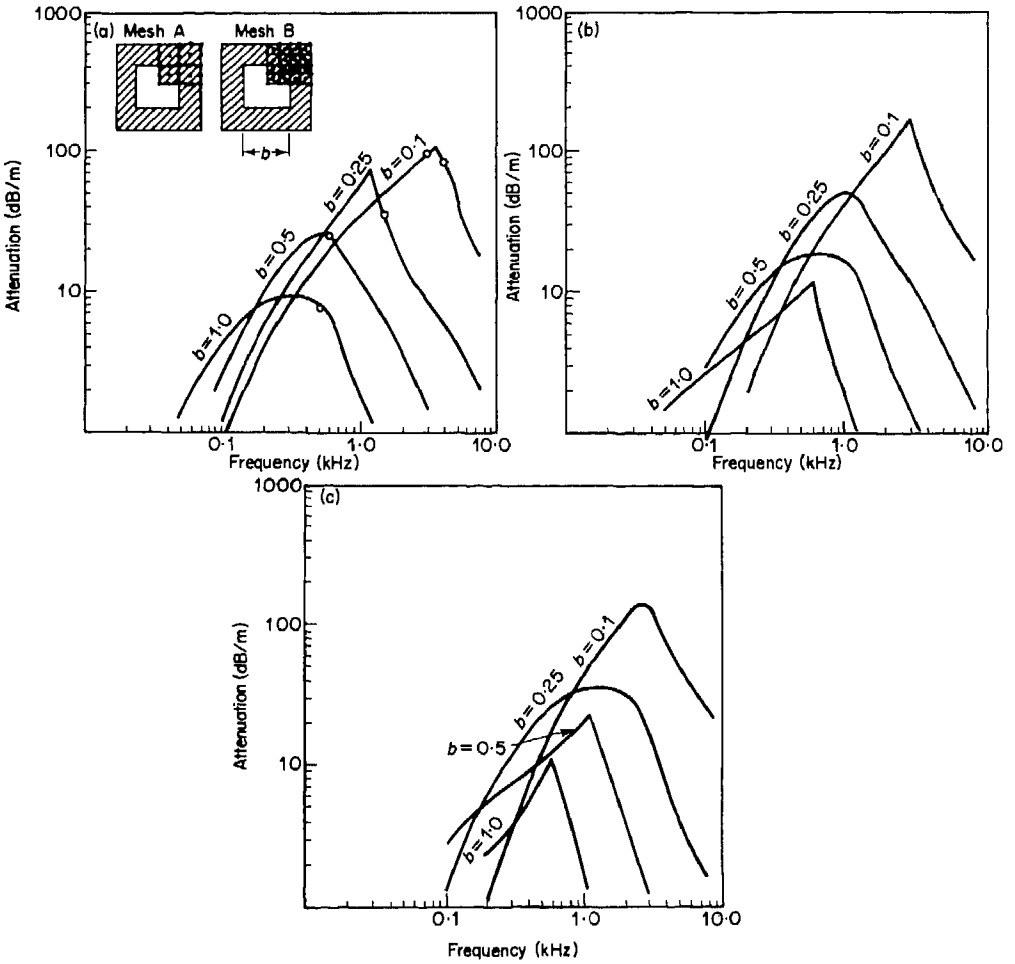

Figure 11. Attenuation of the least attenuated mode in square ducts, 50% space factor; ——, mesh A; O, mesh B; (a) $\sigma = 10^4$ SI rayl/m, (b) $\sigma = 2 \times 10^4$ SI rayl/m, (c) $\sigma = 4 \times 10^4$ SI rayl/m.

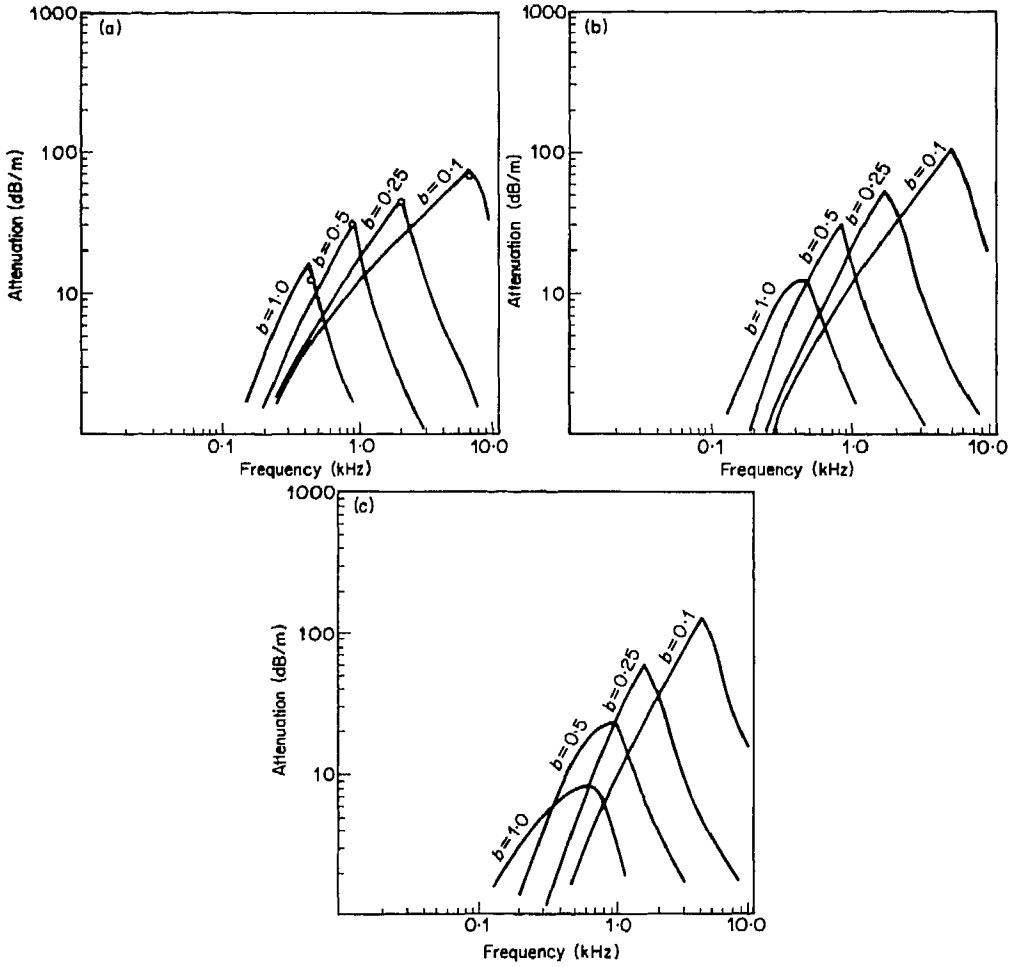

Figure 12. Attenuation of the least attenuated mode in square ducts, 75% space factor; ——, mesh A, O, mesh B; (a) $\sigma = 10^4$ SI rayl/m; (b) $\sigma = 2 \times 10^4$ SI rayl/m; (c) $\sigma = 4 \times 10^4$ SI rayl/m.

"crossing" of two distinct modes as discussed previously (see section 4.2). The overall effect is, however, the same. The occurrence of sharp rather than smooth maxima appears to be somewhat arbitrary and not related directly to duct size or flow resistance but to a combination of the two.

5.2. THE EFFECT OF NON-SQUARE DUCT CROSS-SECTIONS

Although reasonably comprehensive in the range of parameters selected, the charts of section 5.1 refer only to square ducts. To produce similar data for rectangular ducts for a reasonable range of duct aspect ratios would require a substantial number of additional figures. The effect of varying the cross-section from square to rectangular appears to be of somewhat secondary importance, however, certainly for modest values of aspect ratio. This is illustrated by two families of attenuation curves shown in Figure 13. These curves refer to the largest and smallest of the square ducts of section 5.2 (those with airway cross-sections of $0{\cdot}1 \times 0{\cdot}1$ m^2 and $1{\cdot}0 \times 1{\cdot}0$ m^2 respectively) and are presented for a single value of flow resistivity (10 000 SI rayl/m) and space factor (50%). The dotted curves in Figure 13 are obtained by varying the aspect ratio of the airway, b/a, to maintain the

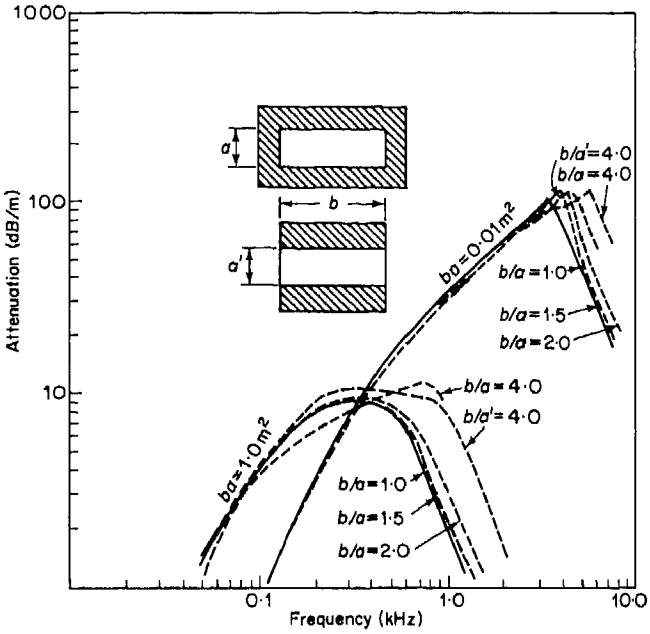

Figure 13. Attenuation of rectangular cross-section ducts, space factor 50%, $\sigma = 10^4$ SI rayl/m.

same airway cross-section (0·01 and 1·0 m^2 respectively) and by adjusting the thickness of the liner so that the same overall cross-sectional area of liner—and hence the same space factor—is retained. Curves are shown for $b/a = 1{\cdot}0$ (square), 1·5, 2·0 and 4·0. An additional curve obtained by placing all of the liner at two opposite sides of the airway is shown for the case $b/a = 4{\cdot}0$.

Several useful observations may be made from Figure 13. First, the effect on a non-square section is small, and may well be of little significance for design purposes—given other sources of imprecision in such calculations—for aspect ratios less than 2·0. The effect for such ratios is merely to shift slightly to the right the attenuation peak of the equivalent square duct. This holds both for the smallest and largest duct and it appears reasonable to assume that it holds also for values of cross-sectional area between these extremes. With regard to more extreme values of the aspect ratio—and results are given for a value of 4·0 which in the context of practical air-moving duct work would come close to a limiting case—the effect is again essentially that of moving to the right the attenuation peak of the square duct without greatly affecting its magnitude. For the purposes of comparison, data are also given in Figure 13 for a flat duct (with an aspect ratio of 4·0) with lining only on the two longer sides. As might be anticipated, the presence or absence of liner on the short sides does not then greatly affect the attenuation. This leads to the conclusion that the equivalent attenuation charts prepared by the second author for the design of ducts lined on two sides only [3] may be used with little error in such cases.

Overall, the effects of a rectangular (rather than square) geometry in ducts lined on all sides is that of shifting to a higher frequency the attenuation peak of an equivalent square duct. In practical terms such effects are relatively small compared with the effects of varying the cross-sectional area itself and might reasonably be neglected altogether in design calculations involving ducts of modest aspect ratios (less than 2·0 say). It can be accommodated in ducts of flatter cross-section by using design data, already available, for ducts lined only on the two longest sides.

5.3. THE EFFECTS OF MEAN FLOW

The effects of mean flow on the attenuation characteristics of ducts lined on all sides are illustrated with reference to the same restricted sets of parameters as used for the study of non-square ducts in the previous section: that is, only the largest and smallest of the previous range of ducts ($b = 0{\cdot}1$ and $1{\cdot}0$ respectively) are considered with a single characteristic flow resistance of 10 000 SI rayl/m. Curves of attenuation for these ducts are presented in Figure 14 for positive and negative Mach numbers of $0{\cdot}1$ and $0{\cdot}2$ (air velocities in air moving ductwork seldom exceed the larger of these values).

The general effect of mean flow, as demonstrated by the attenuation curves of Figure 14, is very similar to that noted by the second author in his study of ducts lined on two sides only (compare Figure 13 of the present paper with Figure 18 of reference [3]). At low frequencies, downstream travelling waves are less strongly attenuated than their upstream propagating counterparts. This situation is reversed once the attenuation peak is passed. The curves of Figure 14 are so similar to those of reference [3] that one may reasonably conclude that the same general behaviour is exhibited for other values of flow resistance.

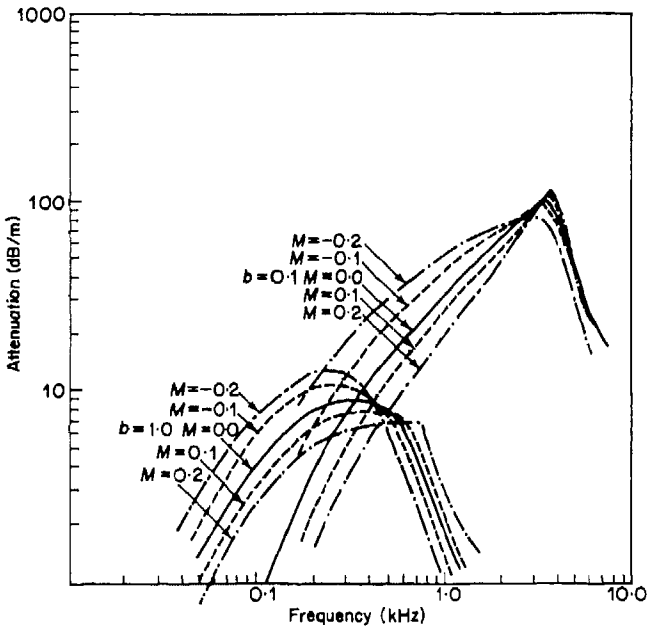

Figure 14. Attenuation in square ducts: the effect of Mach number (space factor 50%, $\sigma = 10^4$ SI rayl/m).

6. DISCUSSION

The finite element numerical scheme presented here, for the calculation of modal attenuation in flow ducts lined with "bulk reacting" acoustically absorbing material, has been shown to yield satisfactory results in comparison to measurements. Identification of the acoustic modes by the customary mode numbers has proven to be less straightforward than it is in hard-walled ducts. This is because the pressure patterns cannot be represented, in the present case, as products of elementary functions and the well-defined transverse nodal lines which characterize hard-wall modes do not always exist in the case of bulk-reacting liners, particularly with even/even modes.

The duct geometry that has been given the most attention in the present study is that of a rectangular duct internally lined on all four sides with porous material. This is not a configuration that is easily amenable to analytical treatment and the use of a numerical method, such as that described here, is appropriate. The finite element formulation in this investigation is, however, sufficiently general that it can be applied to any cross-sectional geometry in a uniform duct, and could thus be applied to ducts of circular or "flat-oval" section, with internal linings.

ACKNOWLEDGMENTS

One of the authors (A.C.) wishes to express his gratitude to the University of Canterbury for financial support in the form of a Visiting Erskine Fellowship, and to the academic and technical staff of the Department of Mechanical Engineering of that University for their invaluable assistance during the experimental tests.

REFERENCES

1. 1984 *ASHRAE Handbook-1984 Systems.* Atlanta: American Society of Heating, Refrigerating and Air Conditioning Engineers Inc. See Chapter 32.
2. I. L. VÉR 1978 *American Society of Heating, Refrigerating and Air Conditioning Engineers Transactions* **84**, 122–149. A review of the attenuation of sound in straight lined and unlined ductwork of rectangular cross section.
3. A. CUMMINGS 1976 *Journal of Sound and Vibration* **49**, 9–35. Sound attenuation in ducts lined on two opposite walls with porous material, with some applications to splitters.
4. R. A. SCOTT 1946 *Proceedings of the Physical Society* **58**, 358–368. The propagation of sound between walls of porous material.
5. R. A. SCOTT 1946 *Proceedings of the Physical Society* **58**, 165–183. The absorption of sound in a homogeneous porous medium.
6. M. E. DELANY and E. N. BAZLEY 1970 *Applied Acoustics* **3**, 105–116. Acoustical properties of fibrous absorbent materials.
7. O. C. ZIENKIEWICZ 1977 *The Finite Element Method.* London: McGraw-Hill Book Company, third edition. See Chapter 3.
8. K. H. HUEBNER 1975 *The Finite Element Method for Engineers.* New York: John Wiley and Sons. See Section 5.8.
9. R. J. ASTLEY and W. EVERSMAN 1979 *Journal of Sound and Vibration* **65**, 61–74. A finite element formulation of the eigenvalue problem in lined ducts with flow.
10. P. M. MORSE and K. U. INGARD 1968 *Theoretical Acoustics.* New York: McGraw-Hill Book Company.